Results in Physics 7 (2017) 1095–1105

Contents lists available at ScienceDirect

Results in Physics

journal homepage: www.journals.elsevier.com/results-in-physics

Structural characterization and colour of $Ni_3V_xP_{2-x}O_8$ ($0 \leq x \leq 2$) and $Ni_2V_yP_{2-y}O_7$ ($0 \leq y \leq 2$) materials

M.A. Tena [a,*], Rafael Mendoza [b], José R. García [c], Santiago García-Granda [b]

[a] Inorganic Chemistry Area, Inorganic and Organic Chemistry Department, Jaume I University, P.O. Box 224, Castellón, Spain
[b] Physical Chemistry Area, Physical and Analytical Chemistry Department, Oviedo University-CINN, Spain
[c] Inorganic Chemistry Area, Organic and Inorganic Chemistry Department, Oviedo University-CINN, Spain

ARTICLE INFO

Article history:
Received 7 January 2017
Received in revised form 14 February 2017
Accepted 15 February 2017
Available online 23 February 2017

Keywords:
Phosphates
Vanadates
Nickel
Structure
Solid solutions
Colour

ABSTRACT

Structural characterization of $Ni_3V_xP_{2-x}O_8$ ($0 \leq x \leq 2$) and $Ni_2V_yP_{2-y}O_7$ ($0 \leq y \leq 2$) compositions was made and colour parameters of these materials measured. Ni(II) diphosphate and divanadate crystalline phases are not stables at high temperature. Solid solutions in $Ni_3P_2O_8$ and $Ni_3V_2O_8$ are obtained by incorporation of V(V) in Ni orthophosphate and P(V) in Ni orthovanadate structures. Solid solutions with $Ni_3V_2O_8$ structure are formed in a greater compositional interval than solid solutions with $Ni_3P_2O_8$ structure. These materials might be used as ceramic pigments because of its thermal and chemical stability. Tan brown colorations were obtained in glazed tiles when the fired compositions were 4% weight enamelled with a commercial glaze.

Introduction

The structure adopted by a particular crystalline material depends, to a first approximation, on three main factors: the general chemical formula and the valences of the elements present, the nature of the bonding between the atoms and the relative size of the atoms or ions. The nature of the bonding between atoms affects considerably the coordination numbers and hence has a major influence on the resulting crystal structure. In non-molecular materials, the valence of an atom or ion does not have a direct bearing on coordination numbers and structure, apart from its obvious importance in controlling the general formula of the compound. The coordination numbers are related directly to the general formula. In a compound $A_xB_yC_z$, in which A and B are cations coordinated only to anions, C, the average cation coordination number (CN) is related to the anion coordination number by: x (CN of A) + y (CN of B) = z (CN of C) [1]. In the case of different crystallographic sites for a cation or for the two cations (A1, A2, B, ...) in the structure, the occupation of crystallographic sites calculated from the multiplicity of positions might be incorporated in the mathematical expression (Multiplicity of each position of a space group is given in International Tables for crystallography [2]). The expression can be extended to include compounds with more complicated general formula and solid solutions by:

$$\sum_{i=1}^{n}[(\text{occupation for cation i}) \cdot (\text{CN of i})] = \sum_{j=1}^{m}[(\text{occupation for anion j}) \cdot (\text{CN of j})]$$

where n is the number of different crystallographic sites occupied by cations and m is the number of crystallographic different sites occupied by anions in the considered structure, when solid solutions are not considered. Summands are added to include cations or anions in the same crystallographic site when solid solutions are considered. In the last case, n or m is the number of crystallographic different sites for cations or anions in the structure including the crystallographic sites partially occupied by ions forming solid solutions.

Vanadium is easily retained in bones. Replacement of phosphorous by the incorporation of vanadium in the inorganic phase of bones ($Ca_{10}(PO_4)_6(OH)_2$) has been suggested in the literature due to the similarity of the chemical behavior of V(V) and P(V) [3]. The size of the V(V) and P(V) is sufficiently different to be replaced each other easily in crystal structures although it might be possible by the formation of solid solutions in reduced ranges of

* Corresponding author.
E-mail addresses: tena@uji.es (M.A. Tena), rafam80@gmail.com (R. Mendoza), jrgm@uniovi.es (J.R. García), s.garciagranda@cinn.es (S. García-Granda).

http://dx.doi.org/10.1016/j.rinp.2017.02.021
2211-3797/

composition. It seems most probably that vanadium-containing compounds can be retained in the cavities of the phases of bones.

Most of divalent metal orthophosphates, $M_3P_2O_8$, crystallize in monoclinic system (M = Mg, Ca, Cr, Mn, Fe, Co, Ni, Zn, Cd, Hg, Pb, Sn) while, usually, the divalent metal orthovanadates, $M_3V_2O_8$, have orthorhombic symmetry (M = Mn, Co, Ni, Zn, Mg), and the divalent metal diphosphates, $M_2P_2O_7$, tend to be polymorphic. Two or more monoclinic crystalline forms are known for some $M_2P_2O_7$ (M = Co, Ni, Cu, Mg) while the monoclinic symmetry is known for some $M_2V_2O_7$ (M = Mn, Co, Ni, Cu, Zn, Mg, Pb, Cd) [4–11]. More detailed structural information can be found as "Supporting Materials".

Ni^{2+} in sixfold coordination in oxides produces green or yellow colours frequently. Bright yellow colour results when Ni^{2+} is in a six-coordinated site significantly distorted from octahedral symmetry. Increased absorption intensity occurs when the metal ion d-d bands are in the proximity to an ultraviolet charge transfer band. Strong charge transfer transitions dominate the tan colour of $Ni_3V_2O_8$ [12]. This yellow-brown colour might be interesting as a ceramic pigment if it is not lost in glazed tiles.

The aim of this study is to investigate the possible formation of solid solutions between $Ni_3P_2O_8$ and $Ni_3V_2O_8$ and/or between $Ni_2P_2O_7$ and $Ni_2V_2O_7$ compounds, the variation of the colour with different amounts of vanadium and phosphorous in these powder samples and to test the colour in samples enamelled with a commercial glaze because the obtained materials (solid solutions or mixture of crystalline phases) might be used by the ceramic industry as a ceramic pigment.

Experimental procedures

$Ni_3V_xP_{2-x}O_8$ ($0 \le x \le 2$) and $Ni_2V_yP_{2-y}O_7$ ($0 \le y \le 2$) compositions were synthesized by the chemical coprecipitation method [13]. The starting materials were $Ni(NO_3)_2{\cdot}6H_2O$ (Panreac, 99%), H_3PO_4 (Merck, 99%) and NH_4VO_3 (Alfa Aesar, 99%). The stoichiometric amount of $Ni(NO_3)_2{\cdot}6H_2O$ and NH_4VO_3 was added on 100 mL of water with vigorous stirring at room temperature. When x or $y \neq 2.0$, a 0.5 M solution of H_3PO_4 in water was added on this aqueous solution of $Ni(NO_3)_2{\cdot}6H_2O$ and NH_4VO_3. After that, an ammonia solution (Scharlau, 25%) was added until pH = 10 and precipitation of materials was obtained. After the co-precipitation process, the materials were dried through IR-irradiation. In this operation, only water is evacuated. As consequence, the Ni:V:P molar ratio of starting materials is preserved. The dry samples were fired at 300, 600, 800, 1000 and 1200 °C for 12 h in each temperature.

The resulting materials were examined with a Panalitycal X-ray diffractometer to study the development of the crystalline phases at different temperatures. A structure profile refinement was carried out by the Rietveld method (Fullprof.2k computer program) [14–16]. Unit cell parameters and interatomic distances (Ni-O and B-O with B = P, V) in orthovanadates and divanadates structures were obtained from fired compositions to investigate the possibility of formation of solid solution in these synthesis conditions. The diffraction patterns were collected running between 5 and 110° 2θ, using monochromatic CuK_α radiation, a step size of 0.02° 2θ and a sampling time of 10 s. The initial structural information was obtained of the Inorganic Crystal Structure Database [4]. Standard cell [13], standard space group, fractional atomic coordinates and other information of crystalline phases in the literature are included in it. Table 1 includes the reference ICSD to every structure. This initial structural information also appears in the references [6–11] for the main structures of this study but often the standard unit cell is not adopted. Dicvol program [17] was used to obtain initial cell parameters in some compositions.

UV–vis-NIR spectroscopy (diffuse reflectance) allows the Ni(II) site and the V(V)-O and Ni(II)-O charge bands in samples to be studied. A Jasco V-670 spectrophotometer was used to obtain the UV–vis-NIR (ultraviolet visible near infrared) spectra in the 200–2500 nm range. In order to test their efficiency as ceramic pigment, the compositions fired at 1000 °C/12 h were 4% weight enamelled with a commercial glaze (SiO_2 – Al_2O_3 – PbO – Na_2O – CaO glaze) onto commercial ceramic biscuits. Many pigments are dissolved in this glaze. The colour of material is lost when this happens. Glazed tiles were fired for 5 min at 1065 °C and their UV–vis-NIR spectra were obtained.

X-Rite spectrophotometer (SP60, an illuminant D65, an observer 10°, and a reference sample of MgO) was used to obtain CIEL*a*b* colour parameters on fired samples: L* is the lightness axis (black (0) → white (100)), a* the green (−) → red (+) axis, and b* is the blue (−) → yellow (+) axis [18]. The measurements were made on powdered samples and on glazed tiles.

Results and discussion

Table 2 shows the crystalline phase evolution with temperature in $Ni_3V_xP_{2-x}O_8$ ($0 \le x \le 2$) and $Ni_2V_yP_{2-y}O_7$ ($0 \le y \le 2$) compositions. Crystalline phases are poorly developed at 600 °C. From $Ni_3V_xP_{2-x}O_8$ compositions, mixtures of $Ni_3P_2O_8$ and $Ni_3V_2O_8$ are present when $0 < x < 2$ at 1000 (Fig. 1) and 1200 °C. At 1200 °C, a single crystalline phase with $Ni_3P_2O_8$ structure is obtained from x = 0 composition but a mixture of $Ni_3V_2O_8$ and $Ni_2V_2O_7$ crystalline phases is obtained from x = 2 composition. The presence of liquid phase during the thermic treatment of this composition (x = 2) could explain these results. $Ni_3V_2O_8$ compound melts incongruently at 1220 °C [19] while the $Ni_3P_2O_8$ compound melts at 1350 °C [20]. Mixtures of of $Ni_3P_2O_8$ and $Ni_3V_2O_8$ crystalline phases are also obtained from compositions with smaller amounts of vanadium (x > 0).

From $Ni_2V_yP_{2-y}O_7$ ($0 \le y \le 2$) compositions, α-$Ni_2P_2O_7$ is the only crystalline phase when y = 0 at T < 1200 °C. At 1200 °C, the $Ni_3P_2O_8$ is detected together with α-$Ni_2P_2O_7$ crystalline phase in composition with y = 0. The melting point of $Ni_2P_2O_7$ is 1395 °C and the presence of liquid occurs at T > 1320 °C in compositions between $Ni_2P_2O_7$ and $Ni_3P_2O_8$ [20].

$Ni_3P_2O_8$ is the majority crystalline phase when T > 600 °C and $0 \le y \le 1.0$ and when $y \ge 1.5$ and $600 \le T \le 800$ °C is $Ni_2V_2O_7$.

Table 1
Structural information of $Ni_3P_2O_8$, $Ni_3V_2O_8$, $Ni_2P_2O_7$ and $Ni_2V_2O_7$.

Structure	ICSD* reference	Crystalline system	Standard unit cell* (Å and degrees)	Standard space group	Z
$Ni_3P_2O_8$	4269	Monoclinic	a = 5.830(2), b = 4.700(2), c = 10.107(4), β = 91.22(2)	P 1 2_1/c 1	2
$Ni_3V_2O_8$	2646	Orthorhombic	a = 5.936(4), b = 11.420(6), c = 8.240(5)	C m c a	4
α-$Ni_2P_2O_7$	27424	Monoclinic	a = 6.9365(2), b = 8.2652(2), c = 8.9725(3), β = 113.754(1)	P 1 2_1/c 1	4
β-$Ni_2P_2O_7$	30433	Monoclinic	a = 6.501(1), b = 8.239(1), c = 4.48(1), β = 104.14(1)	C 1 2/m 1	2
σ-$Ni_2P_2O_7$	100194	Monoclinic	a = 4.475(3), b = 9.913(5), c = 5.212(3), β = 97.46(10)	P 1 2_1/c 1	2
$Ni_2V_2O_7$	2358	Monoclinic	a = 6.515(8), b = 8.303(7), c = 9.350(6), β = 99.86(8)	P 1 2_1/c 1	4

* Refs. [6–11].

Table 2
Evolution of crystalline phases with temperature in $Ni_3V_xP_{2-x}O_8$ ($0 \le x \le 2$) and $Ni_2V_yP_{2-y}O_7$ ($0 \le y \le 2$) fired compositions.

x	T (°C)	Crystalline phases in $Ni_3V_xP_{2-x}O_8$	Crystalline phases in $Ni_2V_yP_{2-y}O_7$
0.00	600	OP(vw)	P(s)
0.50	600	OP(vw), OV(vw)	P(m), V(vw), OP(vw)
1.00	600	OV(w), OP(vw), V(vw)	OP(m), P(w), V(w), OV(vw)
1.50	600	OV(w), V(vw)	V(m), OP(w), OV(w), P(vw)
2.00	600	OV(w), V(vw)	V(m), OV(w)
0.00	800	OP(s), P(vw)	P(s)
0.50	800	OP(s), OV(w), P(vw)	OP(s), OV(m), P(w)
1.00	800	OP(s), OV(s), P(vw)	OP(s), V(w), β P(vw), OV(vw)
1.50	800	OV(s), OP(w)	V(m), OP(m), OV(w), P(vw)
2.00	800	OV(s), V(vw)	V(s), OV(w)
0.00	1000	OP(s)	P(s)
0.50	1000	OP(s), OV(m)	OP(s), P(w), OV(w), V(w)
1.00	1000	OV(s), OP(m)	OP(s), OV(m)
1.50	1000	OV(s), OP(w)	OV(s), OP(m)
2.00	1000	OV(s)	OV(s), V(m)
0.00	1200	OP(s)	P(s), OP(w)
0.50	1200	OP(s), OV(m)	OP(s), P(w), V(w), OV(vw)
1.00	1200	OP(s), OV(s)	OP(s), OV(m)
1.50	1200	OV(s), OP(w)	OV(s), OP(w)
2.00	1200	OV(m), V(vw)	OV(s), V(w)

Crystalline phases: OP = $Ni_3P_2O_8$ (monoclinic), OV = $Ni_3V_2O_8$ (orthorhombic),
P = α-$Ni_2P_2O_7$ (monoclinic), βP = β-$Ni_2P_2O_7$ (monoclinic), V = $Ni_2V_2O_7$ (monoclinic).
Diffraction peak intensity: s = strong, m = medium, w = weak, vw = very weak.

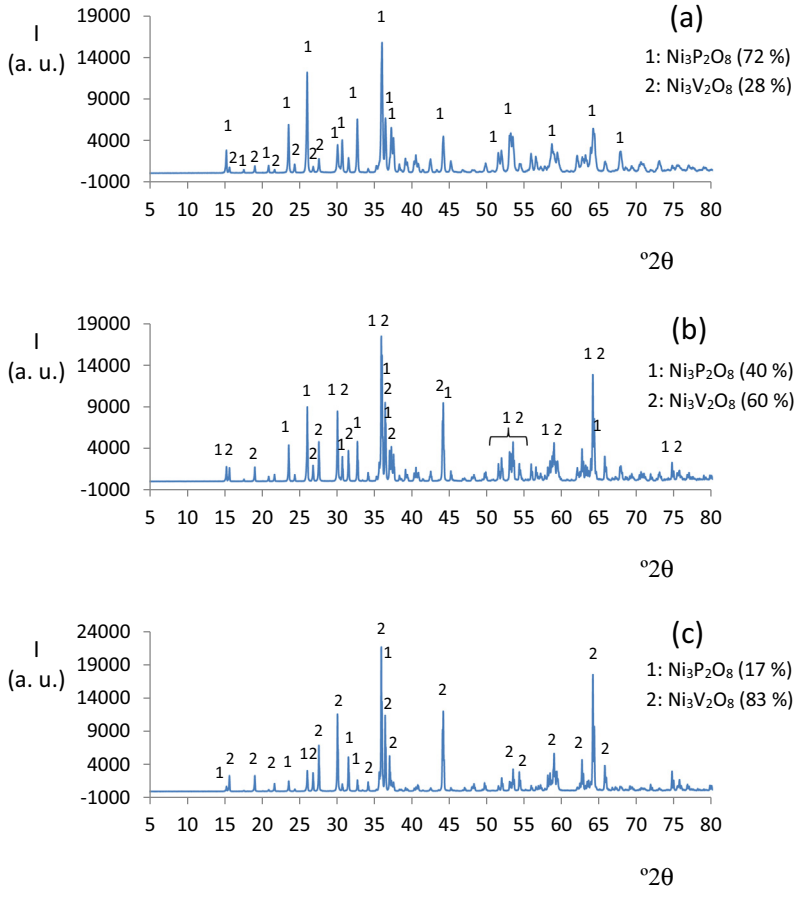

Fig. 1. Diffractograms from $Ni_3V_xP_{2-x}O_8$ compositions fired at 1000 °C, (a) x = 0.5, (b) x = 1.0, (c) x = 1.5.

Mixtures of $Ni_3P_2O_8$ and $Ni_3V_2O_8$ are detected when $0.0 < y < 2.0$ at 1000 °C and 1200 °C.

At 880 °C, $Ni_2V_2O_7$ compound melts incongruently, to give a mixture of $Ni_3V_2O_8$ crystals and liquid because $Ni_3V_2O_8$ is the primary phase. At $880 \le T \le 1190$ °C, the $Ni_3V_2O_8$ cristallizes from the liquid phase [19]. The $Ni_3V_2O_8$ crystalline phase is also detected in conditions of our study (Table 2) when $T \ge 1000$ °C. When $y \ge 1.5$ and $T > 1000$ °C or $y = 2.0$ at 1200 °C, preferred

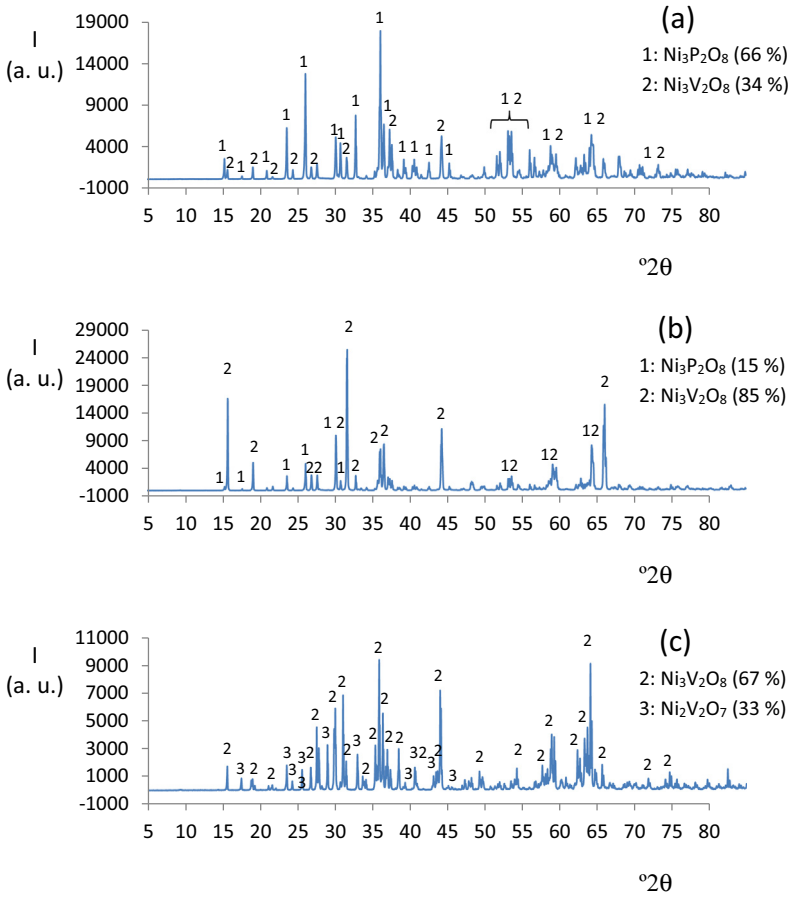

Fig. 2. Diffractograms from $Ni_2V_yP_{2-y}O_7$ compositions fired at 1000 °C. (a) y = 1.0, (b) y = 1.5, (c) y = 2.0.

orientation of $Ni_3V_2O_8$ structure can be observed from the diffraction profile. A strong increase of the three diffraction maxima with hkl 020 (15.4 °2θ), 040 (31.5 °2θ) and 080 (65.7–65.9 °2θ) is detected (Fig. 2b). This fact is in accordance with the crystallization of $Ni_3V_2O_8$ from a liquid phase.

Figs. 3 and 4 show the variation of the standard unit cell parameters in $Ni_3P_2O_8$ and $Ni_3V_2O_8$ structures obtained from $Ni_3V_xP_{2-x}O_8$ ($0 \leq x \leq 2$) samples fired at 1000 °C and 1200 °C. The slight variations of the standard unit cell parameters in $Ni_3P_2O_8$ structure (Table 3a) indicate that only small amounts of V(V) ions are incorporated in this structure (Fig. 3). A decrease of unit cell parameters from $Ni_3V_2O_8$ structure is obtained when $0.5 \leq x \leq 2$ at 800, 1000 and 1200 °C (Table 4a). The variation of these unit cell parameters indicates the formation of solid solutions with $Ni_3V_2O_8$ structure. The decrease of unit cell parameters when x decrease (increase the amount of phosphorus) is in accordance with the replacement of V(V) ion by the smaller P(V) ion in $Ni_3V_2O_8$ structure (Fig. 4). The two points included when y = 1.5 are the unit cell parameters obtained from two crystalline phases with $Ni_3V_2O_8$ structure which diffraction maximum appears at slightly different values of °2θ in high angles. These two phases are solid solutions with this structure and with slightly different compositions (different V/P ratio).

Tables 3–6 show the unit cell parameters and volume in $Ni_3P_2O_8$ (Table 3a and Table 3b), $Ni_3V_2O_8$ (Table 4a and Table 4b), α-$Ni_2P_2O_7$ (Table 5), and $Ni_2V_2O_7$ (Table 6) structures obtained from prepared samples. According to the formation of solid solutions with $Ni_3P_2O_8$ structure, the *c* parameter slightly increases as a consequence of the P/V replacement. However, although the variation in the *a* and *b* parameters is almost irrelevant, the change in the unit cell volume is a more sensitive parameter than the variation in the *c* parameter. The unit cell parameters obtained from α-$Ni_2P_2O_7$ structure (Table 5) are in accordance with the formation of solid solutions when $0 \leq y \leq 0.5$ at 800 and 1000 °C. The substitution of small amount of P(V) ion by V(V) ion produces an slight increase of these values when y increases. The decreasing of unit cell parameters from $Ni_2V_2O_7$ structure when y decreases (Table 6) is in accordance with the formation of solid solutions in this structure when $1.5 \leq y \leq 2.0$ at 600 °C and when $1.0 \leq y \leq 2.0$ at 800 °C. The P(V) ion replaces partially to V(V) ion in Ni(II) ortovanadate and Ni(II) divanadate and only a small amount of V(V) ion replaces to P(V) ion in Ni(II) orthophosphate and α-$Ni_2P_2O_7$ structures.

Figs. 5 and 6 show the variation of the unit cell volume in $Ni_3P_2O_8$ and $Ni_3V_2O_8$ structures from $Ni_3V_xP_{2-x}O_8$ ($0.5 \leq x \leq 2.0$) and $Ni_2V_yP_{2-y}O_7$ ($0.5 \leq y \leq 2.0$) compositions fired at 1000 and 1200 °C. From the variation of volume, the limit of formation of solid solutions can be established about a V:P ratio between 0.75:1.25 and 1.00:1.00 in $Ni_3P_2O_8$ structure and about a V:P ratio = 1.25:0.75 in $Ni_3V_2O_8$ structure.

Fig. 7 shows the variation of the Ni-O and B-O (B = P, V) distances with composition in $Ni_3P_2O_8$ and in $Ni_3V_2O_8$ structures at 1000 °C. In the $Ni_3P_2O_8$ structure, an increase of the B-O (B = P, V) distance can be appreciated when $x \leq 0.75$. This result is in accordance with the substitution of P(V) ion by V(V) ion in this structure, because of the formation of solid solutions in it. A decrease in some Ni-O distances with x can be observed. The formation of solid solutions in $Ni_3P_2O_8$ structure changes the atomic coordinates although the unit cell parameters only change slightly. In the $Ni_3V_2O_8$ structure, the incorporation of P(V) when solid solutions

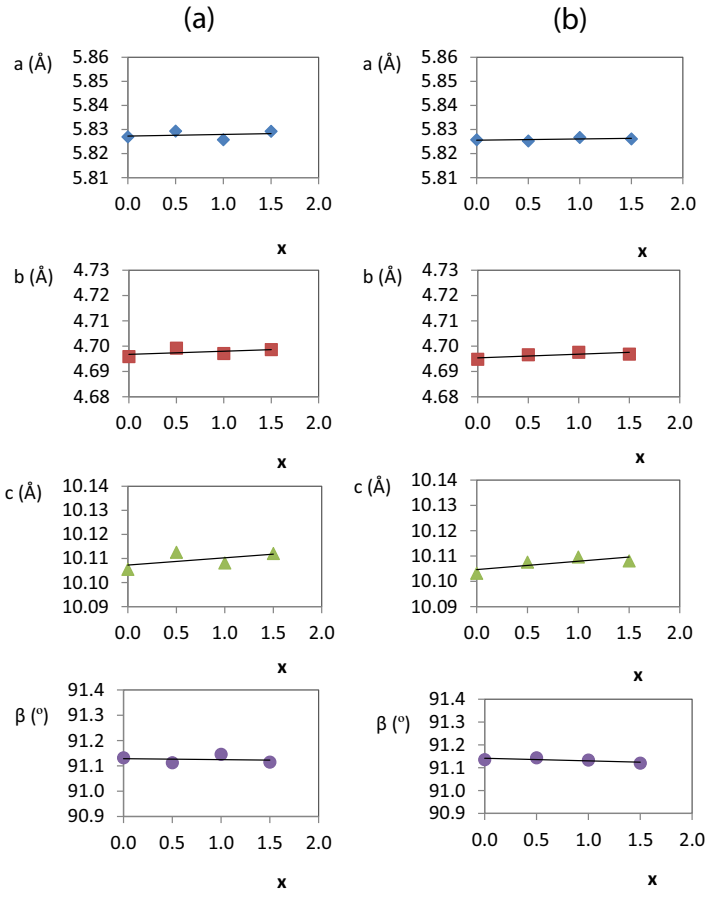

Fig. 3. Variation of unit cell parameters in $Ni_3P_2O_8$ structure from $Ni_3V_xP_{2-x}O_8$ ($0.0 \leq x \leq 1.5$) compositions fired at 1000 °C (a) and 1200 °C (b).

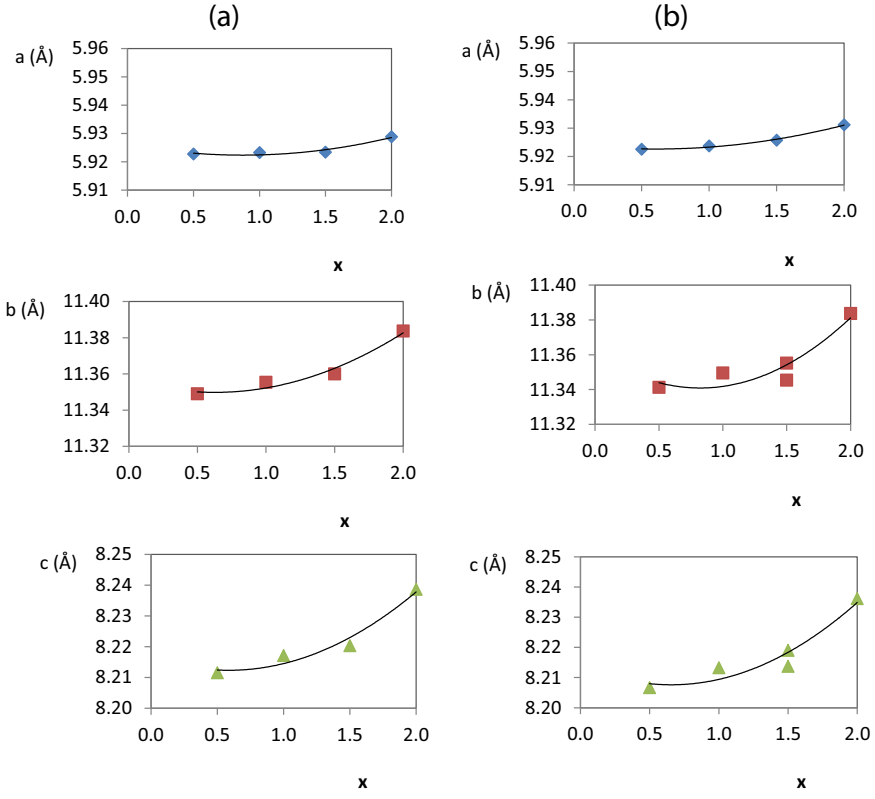

Fig. 4. Variation of unit cell parameters in $Ni_3V_2O_8$ structure from $Ni_3V_xP_{2-x}O_8$ ($0.5 \leq x \leq 2.0$) compositions fired at 1000 (a) and 1200 °C (b).

Table 3a
Unit cell parameters in $Ni_3P_2O_8$ structure from $Ni_3V_xP_{2-x}O_8$ $(0 \le x \le 2)$ fired compositions.

x or y	T (°C)	a(Å)/b(Å)/c(Å)//β(°)//V(Å^3)
0.00	800	5.8275(2) /4.6960(1)/10.1058(1)//91.121(1)//276.45(2)
0.50	800	5.8277(3)/4.7009(2)/10.1155(2)//91.404(1)//276.96(3)
1.00	800	5.8243(1)/4.6976(2)/10.1092(2)//91.101(2)//276.54(2)
1.50	800	5.8294(2)/4.6985(1)/10.110(1)//91.106(2)//276.90(2)
0.00	1000	5.8269(1)/4.6958(1)/10.1052(2)//91.131(1)//276.44(2)
0.50	1000	5.8293(2)/4.6992(2)/10.1125(3)//91.112(2)//276.96(3)
1.00	1000	5.8257(2)/4.6971(3)/10.1081(4)//91.145(3)//276.54(4)
1.50	1000	5.8247(1)/4.6963(1)/10.1066(1)//91.146(1)//276.41(1)
0.00	1200	5.8257(2)/4.6947(2)/10.1029(3)//91.132(2)//276.26(3)
0.50	1200	5.8252(2)/4.6966(2) /10.1075(2)//91.143(3)//276.47(3)
1.00	1200	5.8267(3)/4.6976(3)/10.1096(5)//91.133(2)//276.66(5)
1.50	1200	5.8260(2)/4.6968(2)/10.1081(3)//91.119(3)//276.54(3)

Table 3b
Unit cell parameters in $Ni_3P_2O_8$ structure from $Ni_2V_yP_{2-y}O_7$ $(0 \le y \le 2)$ fired compositions.

x or y	T (°C)	a(Å)/b(Å)/c(Å)//β(°)//V(Å^3)
0.00	800	—————
0.50	800	5.8268(3)/4.6961(2)/10.1058(4)//91.128(2)//276.47(4)
1.00	800	5.8234(2)/4.6937(2)/10.1015(1)//91.142(1)//276.05(2)
1.50	800	5.8257(1)/4.6954(1)/10.1049(2)//91.140(1) //276.35(1)
0.00	1000	—————
0.50	1000	5.8270(2)/4.6954(2)/10.1054(3)//91.139(2)//276.43(3)
1.00	1000	5.8257(1)/4.6971(2)/10.1081(1)//91.145(1)//276.54(2)
1.50	1000	5.8247(2)/4.6963(1)/10.1066(3)//91.146(2)//276.41(2)
0.00	1200	5.8259(1)/4.6958(1)/10.1045(1)//91.138(2)//276.38(1)
0.50	1200	5.8280(2)/4.6972(2)/10.1075(3)// 91.134(2)//276.64(3)
1.00	1200	5.8257(4)/4.6971(3)/10.1081(3)//91.145(3)//276.54(4)
1.50	1200	5.8145(5)/4.6991(4)/10.1107(5)//91.179(3)//276.20(6)

are formed decreases the B-O (B = P, V) distances and the variation of Ni-O distance can be appreciated. Changes in the interatomic distances can be attributed to the distortion of the structure when solid solutions are formed [21]. The decrease of the B-O (B = P, V) distance and the Ni-O distance can be appreciated when $2.0 \ge x \ge 1.25$ at 1000 °C according with the limit of formation of solid solutions about x = 1.25 from $Ni_3V_2O_8$ structure at this temperature. This limit can be also appreciated by a slope change in the variation of unit cell parameters (Fig. 4).

The obtained interatomic distances in $Ni_3P_2O_8$ and in $Ni_3V_2O_8$ structures from $Ni_3V_xP_{2-x}O_8$ $(0 \le x \le 2)$ compositions fired at 1000 and 1200 °C are included in Tables 7 and 8 respectively. The B-O (B = P, V) distance increases with x when x < 1.0 from $Ni_3P_2O_8$ structure and when x > 1.0 from $Ni_3V_2O_8$ structure at 1000 and 1200 °C, according with the replacement of pentavalent ion when solid solutions are formed. From these values, changes of the ranges of formation of solid solutions with $Ni_3P_2O_8$ and $Ni_3V_2O_8$ structures at 1000 and 1200 °C are not detected.

The changes in distances can be associated with structural changes and they are due to changes in bond strength when solid solutions are formed. Interactions between ions could explain the smaller Ni-O distances in $Ni_3V_xP_{2-x}O_8$ $(0.5 \le x \le 1.5)$ than in $Ni_3P_2O_8$.

In $Ni_3V_xP_{2-x}O_8$ $(0 \le x \le 2)$ compositions, a progressive modification of the colour with vanadium amount is obtained when solid solutions are formed.

The three spin allowed transitions of Ni^{2+} in an octahedral site: $^3A_{2g} \rightarrow {}^3T_{2g}(F)$, $^3A_{2g} \rightarrow {}^3T_{1g}(F)$ and $^3A_{2g} \rightarrow {}^3T_{1g}(P)$ generally fall within the ranges 1400–800, 900–500 and 550–370 nm respectively in octahedral systems [22]. In addition two spin forbidden

Table 4a
Unit cell parameters in $Ni_3V_2O_8$ structure from $Ni_3V_xP_{2-x}O_8$ $(0 \le x \le 2)$ fired compositions.

x or y	T (°C)	a(Å)/b(Å)/c(Å)//V(Å^3)
0.50	800	5.8952(2)/11.3393(2)/8.1635(3)//545.71(5)
1.00	800	5.9086(2)/11.3413(3)/8.2080(2)//550.03(5)
1.50	800	5.9251(1)/11.3642(2)/8.2215(3)//553.59(4)
2.00	800	5.9306(2)/11.3816(2)/8.2367(2)//555.97(4)
0.50	1000	5.9225(1)/11.3490(1)/8.2115(2)//551.93(3)
1.00	1000	5.9237(2)/11.3554(2)/8.2171(1)//552.73(3)
1.50	1000	5.9233(1)/11.3535(2)/8.2165(1)//552.56 (3)
2.00	1000	5.9314(1)/11.3844(1)/8.2388(1)//556.33(2)
0.50	1200	5.9228(2)/11.3414(3)/8.2067(3)//551.27(5)
1.00	1200	5.9233(2)/11.3496(2)/8.2133(2)//552.16(4)
1.50	1200	5.9234(1)/11.3525(1)/8.2190(1)//552.69(2)
		5.9234(1)/11.3455(1)/8.2138(1)//552.00(2)
2.00	1200	5.9289(1)/11.3837(1)/8.2362(1)//555.88(2)

Table 4b
Unit cell parameters in $Ni_3V_2O_8$ structure from $Ni_2V_yP_{2-y}O_7$ $(0 \le y \le 2)$ fired compositions.

x or y	T (°C)	a(Å)/b(Å)/c(Å)//V(Å^3)
0.50	800	5.8924(3)/11.6057(4)/8.1629(2)//558.22(6)
1.00	800	5.8352(2)/11.5131(2)/8.20573//551.27(5)
1.50	800	5.8661(1)/11.4989(2)/8.2028(2)//553.31(3)
2.00	800	5.9304(2)/11.3826(2)/8.2334(1)//555.78(3)
0.50	1000	5.8903(2)/11.5178(2)/8.1844(1)//555. 26(3)
1.00	1000	5.9237(1)/11.3554(1)/8.2171(2) //552.73(3)
1.50	1000	5.9228(2)/11.3562(2)/8.2190(1)//552.81(3)
		5.9228(2)/11.3347(2)/8.2085(1)//551.06(3)
2.00	1000	5.9309(1) /11.3815(1)/8.2353(1)//555.90(2)
0.50	1200	5.9039(2)/11.5348(2)/8.2119(2)//559.23(4)
1.00	1200	5.9237(1)/11.3554(1)/8.2171(1)//552.73(2)
1.50	1200	5.9228(2)/11.3552(2)/8.2190(1)//552.76(3)
		5.9228(2)/11.3347(2)/8.2125(1)//551.33(3)
2.00	1200	5.9335(2)/11.3847(1)/8.2404(2)//556.65(4)

Table 5
Unit cell parameters in α-$Ni_2P_2O_7$ structure from $Ni_2V_yP_{2-y}O_7$ $(0 \le y \le 2)$ fired compositions.

y	T (°C)	a(Å)/b(Å)/c(Å)//β(°)//V(Å^3)
0.00	800	6.9340(2)/8.2647(2)/8.9693(2)//113.732(1)//470.52(3)
0.50	800	6.937(1)/8.360(1)/9.031(1)//114.80(4)//475.45(2)
0.00	1000	6.9341(2)/8.2646(2)/8.9693(2)//113.732(1)//470.52(3)
0.50	1000	6.9374(3)/8.3785(3)/8.9856(4)//114.597(2)//474.86(6)
0.00	1200	6.9340(2)/8.2647(1)/8.9693(2)//113.732(2)//470.52(3)
0.50	1200	6.848(1)/8.378(1)/8.953 (1)//114.09(1)//468.92(2)

Table 6
Unit cell parameters in $Ni_2V_2O_7$ structure from $Ni_2V_yP_{2-y}O_7$ $(0 \le y \le 2)$ fired compositions.

y	T (°C)	a(Å)/b(Å)/c(Å)//β(°)//V(Å^3)
1.50	600	6.5006(3)/8.2623(4)/9.3252(4)//100.111(6)//493.09(7)
2.00	600	6.5211(2)/8.2974(4)/9.3632(3)//99.883(4)//499.13(5)
1.00	800	6.5059(3)/8.2728(3)/9.3389(2)//99.988(2)//495.10(5)
1.50	800	6.5113(2)/8.2815(1)/9.3448(1)//99.972(1)//496.34(3)
2.00	800	6.5194(1)/8.2970(1)/9.3620(1)//99.894(1)//498.81(2)
2.00	1000	6.5197(1)/8.2969(1)/9.3609(1)//99.893(1)//498.77(2)

bands are usually quite prominent, one, the transition to ^1E_g near the second spin allowed transition (for common systems with Dq/B near unity), and the second, primarily $^1T_{2g}$ between the sec-

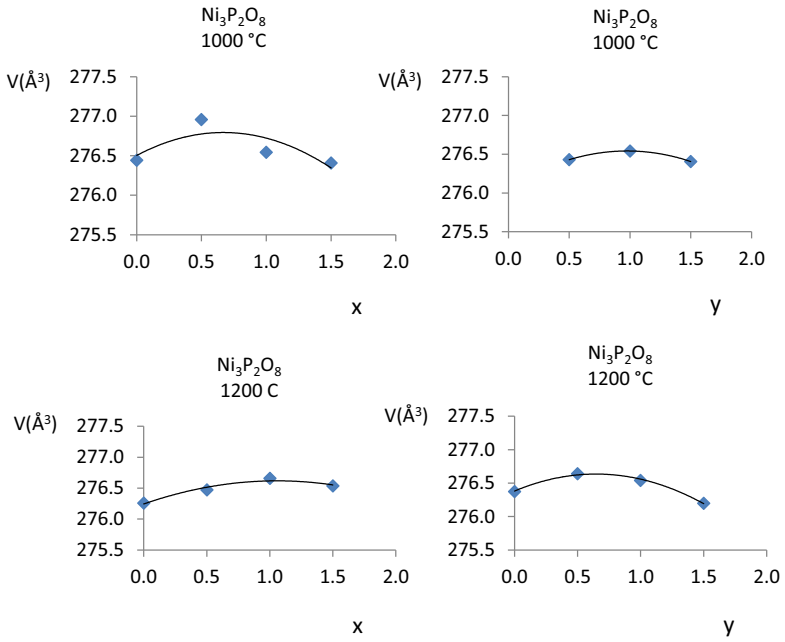

Fig. 5. Variation of unit cell volume in $Ni_3P_2O_8$ structure from $Ni_3V_xP_{2-x}O_8$ ($0.5 \leq x \leq 2.0$) and $Ni_2V_yP_{2-y}O_7$ ($0.5 \leq x \leq 2.0$) compositions fired at 1000 and 1200 °C.

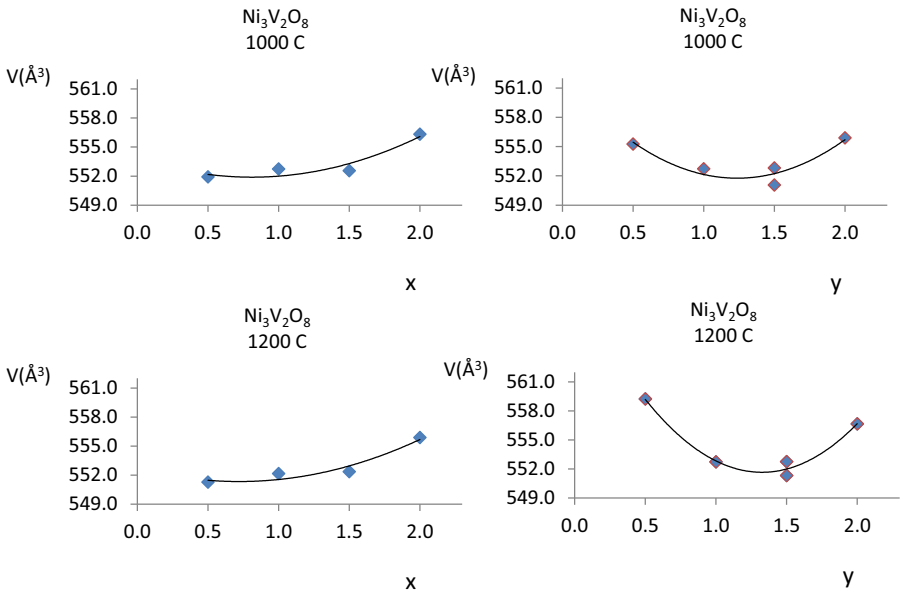

Fig. 6. Variation of unit cell volume in $Ni_3V_2O_8$ structure from $Ni_3V_xP_{2-x}O_8$ ($0.5 \leq x \leq 2.0$) and $Ni_2V_yP_{2-y}O_7$ ($0.5 \leq x \leq 2.0$) compositions fired at 1000 and 1200 °C.

ond and third spin allowed band. The ^1E_g state ($Dq/B \approx 1$) lies so close to $^3T_{1g}$ that extensive mixing takes place leading to observation of a doublet band where the spin forbidden transition has stolen intensity from the spin allowed transition. In a site of low symmetry, the transition to $^3T_{2g}$ is split into up to three components.

In Figs. 8 and 9, the [1000–2500], [600–1100] and [200–650] nm wavelength ranges of the UV-V spectra obtained from $Ni_3V_xP_{2-x}O_8$ ($0 \leq x \leq 2$) and $Ni_2V_yP_{2-y}O_7$ ($0 \leq y \leq 2$) compositions are shown. The three absorption bands are observed about 1250 or 1800 nm (first transition), 700–850 nm (second transition) and 350–550 nm (third transition and charge transfer) from samples fired at T > 800 °C. These bands are assigned to Ni^{2+} in an octahedral site. In this last [200–650] wavelength range are included the absorption band associated with third d-d transition and the charge transfer band of Ni(II)-O and also the V(V)-O charge transfer band. Two facts are noteworthy, the different wavelength for the Ni(II) d-d first transition from rich in P(V) compositions (1800 nm, x or $y \leq 0.5$) and from rich in V(V) compositions (1250 nm, x or $y \geq 1.0$) and the absence of transfer charge band in the visible wavelength range from $Ni_3P_2O_8$ (x = 0) and $Ni_2P_2O_7$ (y = 0) compositions. Both facts are due to the weaker Ni-O bonds when compositions are rich in P(V) because the oxygen between Ni (II) and P(V) are strongly bonded to P(V). The absence of charge transfer in the visible wavelength range in phosphate structures are also reported in $Mg_yCu_{2-y}P_2O_7$ ($0.0 \leq x \leq 1.5$) compositions

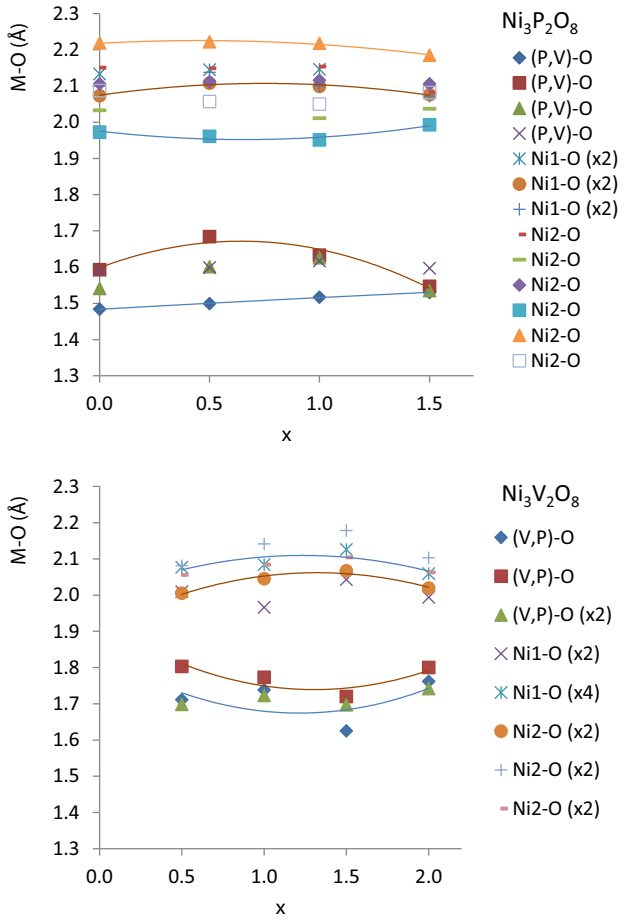

Fig. 7. Variation of the interatomic Ni-O and B-O (B = P, V) distances in $Ni_3P_2O_8$ and $Ni_3V_2O_8$ structures from $Ni_3V_xP_{2-x}O_8$ ($0.0 \leq x \leq 2.0$) compositions fired at 1000 °C.

[21]. From $Ni_3V_xP_{2-x}O_8$ ($0 \leq x \leq 1.5$) compositions, the variation of inflection point between maximum and minimum absorbance in 350–550 nm wavelength range with composition can be observed (Fig. 8). The wavelength in these inflection points increases with the vanadium amount in samples (x). The Ni-O charge transfer band, the V-O charge transfer and the third d-d electronic transition of Ni(II) in an octahedral site are included in these strong absorbance in 350–550 nm wavelength range. An increase of absorbance in 400–650 nm with x is also detected when $T \geq 800$ °C. The variation of inflection point with composition is related to the variation of the Ni-O distances with x ($x > 0$) of the two crystalline phases detected by DRX (Fig. 7). From UV-V spectra of $Ni_3V_xP_{2-x}O_8$ ($0 \leq x \leq 2$) compositions can be also observed the presence of two maximum of absorbance about 750 and 850 nm in Ni(II) second transition band. It might be due to the differences in the second coordination of the Ni(II) in structures.

Table 9 includes the CIE L^* a^* b^* colour parameters and observed colour from $Ni_3V_xP_{2-x}O_8$ ($0 \leq x \leq 2$) and $Ni_2V_yP_{2-y}O_7$ ($0 \leq y \leq 1.5$) fired compositions. At $T \geq 800$ °C, colorations between yellow ($x = 0$ and $y = 0$) and brown ($x = 2$ and $y = 2$) are obtained in $Ni_3V_xP_{2-x}O_8$ ($0 \leq x \leq 2$) and $Ni_2V_yP_{2-y}O_7$ ($0 \leq y \leq 2$) compositions. The strong absorbance in 350–550 nm wavelength range due to charge transfer bands is the most important component in the coloration of samples, just as in the tan colour of $Ni_3V_2O_8$ [12]. This brown colour is also observed in glazed tiles (Table 10). Yellow colorations obtained from $x = 0$ and $y = 0$ change to beige into the commercial glaze used in this study, although this yellow colour is stable into other commercial glazes [13]. From $Ni_3V_xP_{2-x}O_8$ ($0 \leq x \leq 2$) compositions, variations of the tan colour of $Ni_3V_2O_8$ are stable in tested glazed tile although the colour is dark brown when $x \geq 1.5$ (small a^* and b^* values). From $Ni_2V_yP_{2-y}O_7$ ($0 \leq y \leq 2$) compositions beige and greenish colorations are also stable into tested commercial glaze. This fact indicates that these compositions can be used as a ceramic pigment in industry.

Table 7
Interatomic distances in $Ni_3P_2O_8$ structure from $Ni_3V_xP_{2-x}O_8$ ($0 \leq x \leq 2$) compositions fired at 1000 °C and 1200 °C.

Interatomic distances	$Ni_3P_2O_8$ Ref. [6]	T = 1000 °C			
		x = 0.0	x = 0.5	x = 1.0	x = 1.5
B-O	1.521(2)	1.484(2)	1.499(2)	1.517(1)	1.530(1)
(B = P, V)	1.536(2)	1.593(2)	1.684(2)	1.633(1)	1.547(1)
	1.538(2)	1.541(2)	1.601(3)	1.626(1)	1.535(1)
	1.595(2)	1.592(2)	1.599(2)	1.617(1)	1.597(1)
Ni1-O	(x2) 2.098(2)	(x2) 2.133(2)	(x2) 2.145(2)	(x2) 2.146(2)	(x2) 2.088 (2)
	(x2) 2.076(2)	(x2) 2.073 (2)	(x2) 2.108 (2)	(x2) 2.099(2)	(x2) 2.076(2)
	(x2) 2.069(2)	(x2) 2.100(2)	(x2) 2.138(2)	(x2) 2.100(2)	(x2) 2.072(2)
Ni2-O	2.088(2)	2.151(2)	2.149(2)	2.154(2)	2.082(2)
	2.044(2)	2.033(2)	1.973(2)	2.011(2)	2.037(2)
	2.099(2)	2.106(2)	2.112(2)	2.116(2)	2.106(2)
	1.999(2)	1.973(2)	1.961(2)	1.951(2)	1.993(2)
	2.190(2)	2.219(2)	2.222(2)	2.218(2)	2.185(2)
	2.083(2)	2.087(2)	2.057(2)	2.050(2)	2.082(2)
		T = 1200 °C			
B-O	1.521(2)	1.494(2)	1.498(2)	1.518(1)	1.530(1)
(B = P, V)	1.536(2)	1.648(2)	1.683(2)	1.618(1)	1.547(1)
	1.538(2)	1.606(2)	1.601(3)	1.636(1)	1.535(1)
	1.595(2)	1.606(2)	1.596(2)	1.584(1)	1.597(1)
Ni1-O	(x2) 2.098(2)	(x2) 2.148(2)	(x2) 2.144(2)	(x2) 2.143(2)	(x2) 2.088(2)
	(x2) 2.076(2)	(x2) 2.084(2)	(x2) 2.106(2)	(x2) 2.101(2)	(x2) 2.077(2)
	(x2) 2.069(2)	(x2) 2.090(2)	(x2) 2.136(2)	(x2) 2.128(2)	(x2) 2.072(2)
Ni2-O	2.088(2)	2.152(2)	2.148(2)	2.181(2)	2.083(2)
	2.044(2)	2.047(2)	1.972(2)	2.007 (2)	2.037 (2)
	2.099(2)	2.124(2)	2.110(2)	2.086(2)	2.107(2)
	1.999(2)	1.969(2)	1.960(2)	1.978(2)	1.993(2)
	2.190(2)	2.215(2)	2.221(2)	2.255(2)	2.185(2)
	2.083(2)	2.050(2)	2.056(2)	2.028(2)	2.082(2)

Table 8
Interatomic distances in $Ni_3V_2O_8$ structure from $Ni_3V_xP_{2-x}O_8$ ($0 \leq x \leq 2$) compositions fired at 1000 and 1200 °C.

Interatomic distances	T = 1000 °C				$Ni_3V_2O_8$ [Ref. 7]
	x = 0.5	x = 1.0	x = 1.5	x = 2.0	
B-O	1.711(2)	1.738(2)	1.625(2)	1.762(2)	1.722(2)
(B = P, V)	1.803(3)	1.773(4)	1.720(2)	1.800(2)	1.813(2)
	(x2) 1.698(2)	(x2) 1.723(2)	(x2) 1.697(2)	(x2) 1.742(2)	(x2) 1.704(2)
Ni1-O	(x2) 2.009(2)	(x2) 1.966(2)	(x2) 2.043(2)	(x2) 1.994(2)	(x2) 2.017(2)
	(x4) 2.077(2)	(x4) 2.084(2)	(x4) 2.126(2)	(x4) 2.059(2)	(x4) 2.084(2)
Ni2-O	(x2) 2.005(2)	(x2) 2.045(1)	(x2) 2.067(2)	(x2) 2.019(2)	(x2) 2.013(2)
	(x2) 2.081(2)	(x2) 2.141(1)	(x2) 2.178(2)	(x2) 2.103(2)	(x2) 2.091(2)
	(x2) 2.056(2)	(x2) 2.084(1)	(x2) 2.104(2)	(x2) 2.063(2)	(x2) 2.064(2)
	T = 1200 °C				
B-O	1.714(2)	1.738(2)	1.624(2)	1.718(2)	1.722(2)
(B = P, V)	1.803(2)	1.773(2)	1.719(2)	1.810(2)	1.813(2)
	(x2) 1.698(2)	(x2) 1.723(2)	(x2) 1.697(2)	(x2) 1.701(2)	(x2) 1.704(2)
Ni1-O	(x2) 2.009(2)	(x2) 1.966(1)	(x2) 2.043(2)	(x2) 2.016(1)	(x2) 2.017(2)
	(x4) 2.077(2)	(x4) 2.084(1)	(x4) 2.126(2)	(x4) 2.081(1)	(x4) 2.084(2)
Ni2-O	(x2) 2.005(2)	(x2) 2.045(2)	(x2) 2.066(1)	(x2) 2.010(1)	(x2) 2.013(2)
	(x2) 2.081(2)	(x2) 2.141(2)	(x2) 2.178(1)	(x2) 2.087(1)	(x2) 2.091(2)
	(x2) 2.056(2)	(x2) 2.084(2)	(x2) 2.104(1)	(x2) 2.063(1)	(x2) 2.064(2)

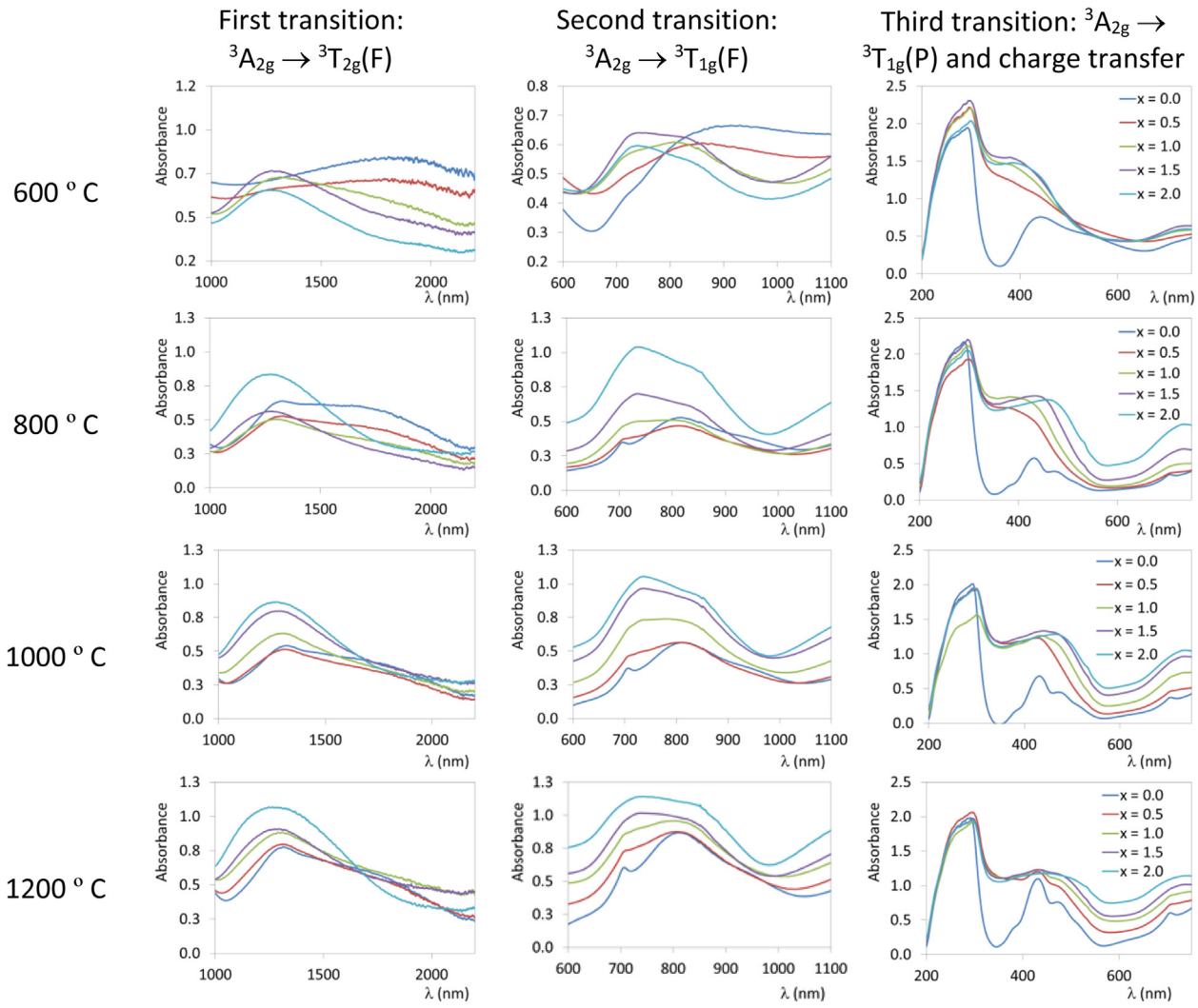

Fig. 8. d-d electronic transitions of Ni(II) in an octahedral site from $Ni_3V_xP_{2-x}O_8$ compositions.

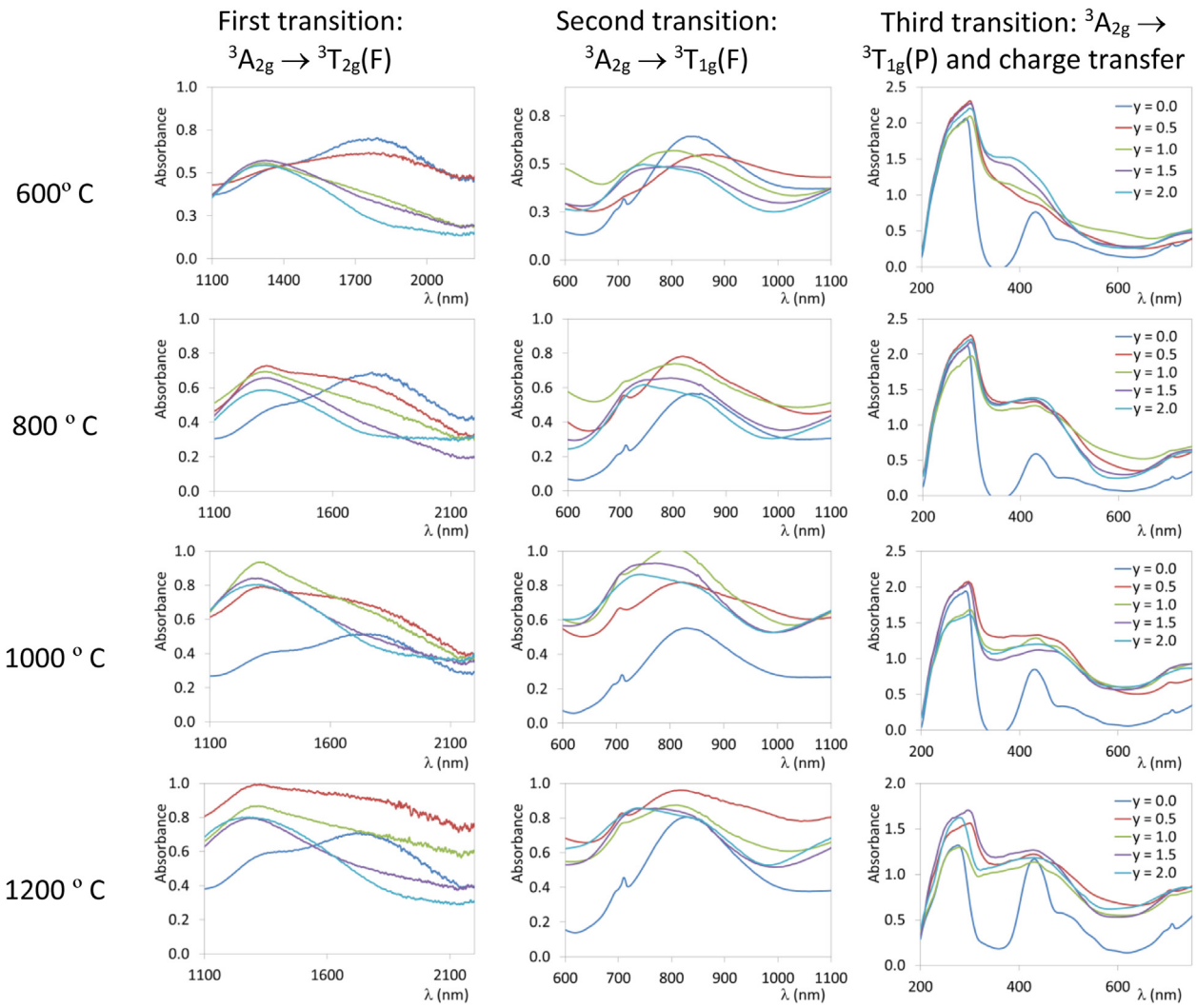

Fig. 9. d-d electronic transitions of Ni(II) in an octahedral site from $Ni_2V_yP_{2-y}O_7$ compositions.

Table 9
CIE L^* a^* b^* colour parameters and observed colour in $Ni_3V_xP_{2-x}O_8$ ($0 \leq x \leq 3$) and $Ni_2V_yP_{2-y}O_7$ ($0 \leq y \leq 2$) fired compositions.

T (°C)	x, y	$Ni_3V_xP_{2-x}O_8$ $L^*/a^*/b^*$ (Observed colour)	$Ni_2V_yP_{2-y}O_7$ $L^*/a^*/b^*$ (Observed colour)
300	0.00	68.58/7.91/21.84 (beige)	72.04/6.99/27.05 (beige)
300	0.50	64.92/5.74/22.92 (beige)	66.29/8.64/29.56 (beige)
300	1.00	40.51/2.81/11.31 (brown)	62.47/12.01/31.19 (greenish brown)
300	1.50	48.23/2.57/11.23 (brown)	55.61/8.96/24.55 (greenish brown)
300	2.00	47.09/2.33/10.87 (brown)	58.80/8.17/28.51 (greenish brown)
600	0.00	70.18/7.81/19.21 (dark brown)	83.13/3.48/31.65 (yellow pale)
600	0.50	64.89/5.24/22.44 (dark brown)	73.83/6.32/30.61 (yellow-beige)
600	1.00	66.28/3.57/31.69 (orange)	67.49/1.74/23.91 (green)
600	1.50	65.80/3.27/34.54 (yellow)	75.04/2.25/39.60 (yellow)
600	2.00	66.95/1.19/36.40 (light yellow)	76.44/4.03/47.81 (yellow)
800	0.00	68.58/7.91/21.84 (light yellow)	89.10/2.02/29.02 (yellow)
800	0.50	64.92/5.74/22.92 (yellow)	64.65/13.89/36.05 (beige-orange)
800	1.00	40.51/2.81/11.31 (yellow)	59.90/7.95/25.36 (beige)
800	1.50	48.23/2.57/11.23 (yellow)	71.12/9.57/45.24 (yellow)
800	2.00	47.09/2.33/10.87 (beige)	73.71/9.98/51.45 (yellow)
1000	0.00	87.78/-1.54/35.21 (yellow pale)	87.32/3.85/38.46 (bright yellow)
1000	0.50	81.63/0.79/56.01 (yellow)	59.66/11.46/27.07 (reddish beige)
1000	1.00	72.90/5.98/49.66 (yellow brown)	58.50/7.38/23.41 (greenish beige)
1000	1.50	64.97/7.28/38.75 (tan brown)	59.59/6.67/23.64 (greenish brown)
1000	2.00	60.86/7.22/29.15 (tan brown)	59.79/5.21/24.78 (brown)
1200	0.00	82.49/0.69/47.31 (lemon yellow)	80.14/9.52/46.06 (bright yellow)
1200	0.50	71.24/5.55/40.05 (mustard yellow)	56.26/5.26/19.43 (brown)
1200	1.00	63.73/6.28/29.70 (beige)	61.49/4.09/27.12 (greenish brown)
1200	1.50	59.62/6.79/26.54 (tan brown)	62.24/4.80/29.47 (greenish)
1200	2.00	54.77/4.89/14.08 (tan brown)	57.62/3.04/19.69 (greenish)

Table 10
CIE $L^* a^* b^*$ colour parameters in $Ni_3V_xP_{2-x}O_8$ ($0 \le x \le 3$) and $Ni_2V_yP_{2-y}O_7$ ($0 \le y \le 2$) compositions fired at 1000 °C from glazed tiles.

x, y	$Ni_3V_xP_{2-x}O_8$ $L^*/a^*/b^*$	$Ni_2V_yP_{2-y}O_7$ $L^*/a^*/b^*$
0.00	46.51/8.76/22.46	49.63/12.74/28.87
0.50	41.81/6.21/13.34	50.02/7.67/23.05
1.00	38.63/5.89/11.52	43.55/6.39/16.04
1.50	37.27/4.02/8.01	40.99/6.31/14.89
2.00	37.55/2.92/6.12	54.43/5.39/14.11

Conclusions

Structural characterization of precipitates with $Ni_3V_xP_{2-x}O_8$ ($0 \le x \le 2$) and $Ni_2V_yP_{2-y}O_7$ ($0 \le y \le 2$) compositions were performed and the results are presented. The presence of liquid phase during the thermic treatment of the prepared compositions explains the development of crystalline phases in them. Mixtures of $Ni_3P_2O_8$ and $Ni_3V_2O_8$ are present when $0 < x < 2$ at 1000 and 1200 °C. The decreasing of unit cell parameters when x decrease (increasing the amount of phosphorus) is in accordance with the replacement of V(V) ion by the smaller P(V) ion in $Ni_3V_2O_8$ structure. The slight variations of the standard unit cell parameters in $Ni_3P_2O_8$ structure indicate that only small amounts of V(V) ions are incorporated in this structure. The variation of the unit cell volume allows to establish the limits of formation of solid solutions with $Ni_3P_2O_8$ structure about $x = 0.75$ and with $Ni_3V_2O_8$ structure about $x = 1.25$ at 1000 and 1200 °C/1 h. The Ni(II) diphosphate and Ni(II) divanadate solid solutions are obtained but they are not stables when temperature increases.

The different ratio of the crystalline phases modifies the coloration of the studied samples. The strong absorbance in 350–550 nm wavelength range is the most important component in the coloration of samples, just as in the tan colour of $Ni_3V_2O_8$. The Ni-O charge transfer band, the V-O charge transfer and the third d-d electronic transition of Ni(II) in an octahedral site are included in these strong absorbance.

Colour of materials is not lost when they are enamelled with a commercial glaze onto commercial ceramic biscuits. These new materials are suitable to be used as a ceramic pigment.

Acknowledgement

We gratefully acknowledge the financial support given by MINECO, MAT2013-40950-R project, ERDF funding and MAT2016-78155-C2-1-R project.

References

[1] West AR. Solid State chemistry and its applications. Chichester: John Wiley & Sons; 1984. p. 265.
[2] International Tables for Crystallography, Volume A: Space-Group Symmetry. Fifth Edition 2002. Published for The International Union of Crystallography by Kluwer Academic Publishers. London; 2004.
[3] Baran Enrique J. Química bioinorgánica. Madrid, España: McGraw-Hill; 1995. p. 166–70.
[4] Inorganic Crystal Structure Database (ICSD). Fachinformationszentrum (FIZ, Karlsruhe, Germany); 2014.
[5] Durif A. Crystal chemistry of condensed phosphates. New York: Plenum Press; 1995. Chapter 2.
[6] Calvo C, Faggiani R. Structure of nickel orthophosphate. Can J Chem 1975;53:1516–20.
[7] Sauerbrei EE, Faggiani R, Calvo C. Refinement of the crystal structures of $Co_3V_2O_8$ and $Ni_3V_2O_8$. Acta Cryst 1973;B29:2304–6.
[8] Łukaszewicz K. Crystal structure of a-$Ni_2P_2O_7$. Bulletin de L'Académie Polonaise des Sciences. Serie des Sciences Chimiques 1967;XV(2):47–51.
[9] Pietraszko A, Łukaszewicz K. Crystal structure of β-$Ni_2P_2O_7$ determined on a weissenberg goniometer with a high-temperature attachment. Bulletin de L'Académie Polonaise des Sciences, Serie des Sciences Chimiques 1968;4 (4):183–7.
[10] Masse R, Guitel JC, Durif A. Structure crystalline d'une nouvelle variete de pyrophosphate de nickel: $Ni_2P_2O_7$. Mater Res Bull 1979;14:337–41.
[11] Sauerbrei EE, Faggiani R, Calvo C. Cobalt vanadate, $Co_2V_2O_7$, and nickel vanadate, $Ni_2V_2O_7$. Acta Cryst 1974;B30:2907–9.
[12] Rossman GR, Shannon RD, Waring RK. Origen of the yellow color of complex oxides. J Solid State Chem 1981;39:277–87.
[13] Tena MA. Characterization of $Mg_xM_{2-x}P_2O_7$ (M = Cu and Ni) solid solutions. J Eur Ceram Soc 2012;32(2):389–97. http://dx.doi.org/10.1016/j.jeurceramsoc.2011.09.018.
[14] Rietveld HM. A profile refinement method for nuclear and magnetic structures. J Appl Cryst 1969;2:65–71.
[15] Rodriguez-Carvajal J, (January 2015-ILL-JRC), Fullprof. 2k computer program, version 5.60, France.
[16] Laurent Chapon (Rutherford Appleton Laboratory, UK) and Juan Rodriguez-Carvajal (Institut Laue Langevin, France) (August 2008). FPStudio computer program, version 2.0.
[17] Boultif A (Algeria), Loüer D. (Rennes 1 university, France). Dicvol computer program, version 06 (November 2007).
[18] Commission Internationale del'Eclairage (1978), Recommendations on Uniform Color Spaces, Color Difference Equations, Phychometrics Color Terms, Supplement n° 2 of CIE Publication N° 15 (E1–1.31). Bureau Central de la CIE, Paris; 1971.
[19] Brisi Cesare. I sistemi ossido di nichel-anidride vanadica e ossido di cobalto-anhidride vanadica. Ann Chim (Rome) 1957;47:806–16 [7, 8].
[20] Levin Ernest M, McMurdie Howard F. Phase diagrams for ceramist, Am Ceram Soc, cop; 1956–1959. Figure 2325.
[21] Tena MA, García-Granda Santiago. Structural characterization and colour of $MgxCu_3{-}xV_2O_8$ ($0 \le x \le 3$) and $MgyCu_2{-}yV_2O_7$ ($0 \le y \le 2$) compositions. Springer Plus 2015;4(163):1–17. http://dx.doi.org/10.1186/s40064-015-0908-8. http://www.springerplus.com/content/4/1/163.
[22] Lever ABP. Inorganic electronic spectroscopy. The Netherlands: Elsevier Science B. V.; 1977. 507-511.